Proceedings of IMECE 07
2007 ASME International Mechanical Engineering Congress and Exposition
November 10-16, 2007, Seattle, USA

IMECE2007-43779

CFD COMPUTATION OF FAN INTERACTION NOISE

Sheryl M. Grace*
Department of Aerospace
and Mechanical Engineering
Boston University
110 Cummington St.
Boston, MA 02215
Email: sgrace@bu.edu

Douglas L. Sondak
Scientific Computing
and Visualization
Boston University
Boston, MA, 02215
Email: sondak@bu.edu

Daniel J. Dorney
Team Lead, Fluid Dynamics Branch
NASA Marshall Space Flight Center
Marshall Space Flight Center, AL 35812
Email: daniel.j.dorney@nasa.gov

Michaela Logue
Aerospace and Mechanical Engineering Department
The University of Notre Dame
Notre Dame, IN 45665
Email: mlogue@nd.edu

ABSTRACT

In this study, a 3-D, unsteady, Reynolds-averaged Navier-Stokes (RANS) CFD code coupled to an acoustic calculation is used to predict the contribution of the exit guide vanes to tonal fan noise downstream. The configuration investigated is that corresponding to the NASA Source Diagnostic Test (SDT) 22-in fan rig. One configuration from the SDT matrix is considered here: the approach condition, and outlet guide vane count designed for cut-off of the blade passage frequency. In this chosen configuration, there are 22 rotor blades and 54 stator blades. The stators are located 2.5 tip chords downstream of the rotor trailing edge. The RANS computations are used to obtain the spectra of the unsteady surface pressure on the exit guide vanes. The surface pressure at the blade passage frequency and its second harmonic are then integrated together with the Green's function for an annular duct to obtain the pressure at locations in the duct. Comparison of the computed sound power level at the exhaust plane with experiment show good agreement at the cut-on circumferential mode. The results from this investigation validate the use of the CFD code along with the acoustic model for downstream fan noise predictions. This validation enables future investigations such as the effect of duct variation on the exhaust tonal power level and the validity of using this method for predicting broadband noise levels.

NOMENCLATURE

$\beta = \sqrt{1-M^2}$ compressibility parameter
ω radial frequency of disturbance
a outer radius of annulus
c chordlength
c_0 mean speed of sound
h inner radius of annulus
I acoustic intensity
g gust amplitude, 2D benchmark simulation
G Green's function
J_n, Y_n Bessel functions of order n
$k = \omega/c_0$ acoustic wave number
k_1, k_2 nondimensional wave numbers of 2D gust
K_{nm} eigenfrequencies of propagation
M Mach number

*Address all correspondence to this author.

Copyright © 2007 by ASME

p pressure
$\mathcal{P}$ acoustic power
q, s integers, multipliers of B and V
r_h, r_t, r radial location of rotor hub, tip, strip
u acoustic velocity in the axial direction
$(x, y, z), (r, \theta, z)$ point in space
$\mathbf{x_0} = (r_0, \theta_0, z_0)$ source locations

INTRODUCTION

One source of fan noise is the interaction of rotor wake flow with downstream exit guide vanes (EGV). The contribution of this rotor-stator interaction to fan noise was investigated at NASA experimentally using an 22-in fan rig designed specifically for noise assessment of turbofans [1, 2].

Fan noise consists of both tonal and broadband elements. The long term goal of the current research is to assess the viability of using CFD in a prediction method for fan broadband noise. However, the first phase of the research presented in this paper, focused on the use of CFD in the prediction of tonal noise.

Previous studies of fan noise have focused on analytically modeling the inflow (i.e., rotor wakes) [3, 4] and determining the unsteady response of the exit guide vanes to the inflow via a cascade model. The cascade calculations have varied from semi-analytical approaches valid for two-dimensional, unloaded, flat-plate cascades [5], to flat-plate cascades used in conjunction with a strip theory [6, 7], to computational and asymptotic solutions of the linearized Euler equations for two-dimensional cascades with a real blade section geometry [8–10].

The acoustic field produced by the exit guide vane is then computed as a second step via Green's method [4, 8, 11, 12] or another suitable acoustic calculation process [13, 14]. Most studies use canonical shapes for the duct such as an infinite cylinder or an infinite annulus and assume axial flow in the duct. Cooper and Peake [15], however, have introduced a method for incorporating real duct geometry in the acoustic calculation, and others [16–18] have considered the inclusion of swirling flow.

More recently, Nallasamy and Envia [19] used CFD to define the inflow to the exit guide vane. They computed the rotor wakes, taking into account the downstream vanes, using the average passage code APNASA. These wakes were used to describe the inflow to a flat-plate exit guide vane configuration representing the real exit guide vanes. A strip theory analysis of the flat-plate EGV response provided the unsteady surface pressure on the vanes that was used to compute the acoustic field via the Green's method for propagation in an infinite cylinder.

This research aims at extending the work by Nallasamy and Envia in two ways. First, a 3-D, unsteady, Reynolds-averaged Navier-Stokes CFD code is used to predict the fully coupled turbomachinery flow field and vane surface pressures. The CFD code has been used extensively for turbomachinery flow simulations. One such example that is relevant to the current study is its use in predicting clocking effects in an axial compressor [20]. The rotor wake prediction from this fully coupled CFD simulation is compared to the experimental results and also to the prediction obtained using the average passage assumption described in [19]. Second, the unsteady vane pressure computed via CFD is used as input to the Green's method to obtain the acoustic prediction.

The NASA Source Diagnostic Test (SDT) was chosen as the focus of this computational study mainly because of its systematic variation of geometric and flow parameters that affect turbofan noise. For instance, the test matrix includes results for various operating conditions, a rotor-alone configuration and three rotor-stator configurations in which the outlet guide vane design varies. In addition, it allows for direct comparison with the previous results of Nallasamy and Envia [19].

In this paper, one configuration from the SDT matrix is studied: the approach condition with outlet guide vane count designed for cut-off of the blade passage frequency. In the chosen configuration there are 22 rotor blades and 54 exit guide vanes. The vanes are located 2.5 tip chords downstream of the rotor trailing edge. Unfortunately, for this configuration, the vanes were too thin to be outfitted with pressure taps and thus there are no experimental surface pressure data with which to compare our surface pressure results. The final result for the sound power level at the exhaust plane agrees well with the measured values.

The computational method used for the flow simulation is described in the next section. The acoustic calculation method is then described and the results for the STD case are discussed.

CFD METHOD

The flow field simulation has been performed using Phantom, a time-dependent, three-dimensional Reynolds-averaged Navier-Stokes solver for turbomachinery [21,22]. This code uses the General Equation Set method, which is applicable to ideal and real fluids for both compressible and incompressible flows [23]. It employs an implicit, time-marching, finite-difference scheme that is third-order accurate in space and second-order accurate in time. The inviscid fluxes are discretized using Roe's scheme [24], and the viscous fluxes are calculated using standard central differences. Approximate-factorization is used along with dual time-stepping, which minimizes factorization errors. The turbulent viscosity is calculated using the Baldwin-Lomax algebraic turbulence model [25].

The solver uses O and H-type zonal grids to discretize the flow field and facilitate relative motion of the blades and vanes. The O-grids are body fitted to the surfaces of the blades and generated using an elliptic equation solution procedure. They give good resolution at the leading and trailing edges of the blades, and make it easy to apply the turbulence model. Algebraically generated H-grids are used to discretize the remainder of the flow field. Further details on the numerical procedure can be found

Copyright © 2007 by ASME

in [21].

Boundary Conditions

At the inlet, the total pressure, total temperature and the circumferential and radial flow angles are specified, and the upstream-running Riemann invariant is extrapolated from the interior of the computational domain. At the exit, the circumferential and radial velocity components, entropy, and the downstream-running Reimann invariant are extrapolated from the interior of the computational domain. The exit static pressure is specified at the mid-span of the computational exit, and the pressure values at all other radial locations are obtained by integrating the radial equilibrium equation. Periodicity is enforced along the outer boundaries of the H-grids in the circumferential direction.

No-slip boundary conditions are enforced at the hub and tip end walls, and along the airfoil surfaces. It is assumed that the normal derivative of the pressure is zero at the solid wall surfaces, and that the walls are adiabatic.

The flow variables at zonal boundaries are explicitly updated after each time step by interpolating values from adjacent grids.

CFD validation

The turbomachinery code used in this research has been extensively validated in the past on a wide variety of configurations [20, 26, 27]. In particular, the compressor clocking simulations discussed in [20] show that the code can accurately simulate wake interaction. While prior comparisons of simulations using this turbomachinery code have all shown excellent agreement with experiment, it has never been used for aeroacoustic predictions. The method used here for aeroacoustic prediction is extremely sensitive to the accuracy of the unsteady surface pressure distribution on the vanes. While the case discussed in this paper does not allow for comparison of the unsteady surface pressure between experiment and computation, a second case from the NASA STD study does. As such, this comparison is planned for the next stage of this work.

Current Simulation

The current simulation was performed for the approach condition, with a corrected fan speed of 7808 RPM, for the rig configuration with 22 rotor blades and 54 stator blades. The simulation geometry included 2 rotor blades and 5 stator blades, with the stator geometry scaled by 54/55 to maintain the correct blockage. The actual tip clearance from the experiment was not available, so a value of 1% span was assumed.

A total of 18 grids were used in the simulation: 2 H-grids for the inlet duct, an O, H, and clearance grid for each rotor blade, and an o and h grid for each stator blade. Table1 shows the grid densities. The H-grid dimensions are given as axial, circumferential, and spanwise respectively, and the O-grid and clearance-grid dimensions are given as around-the-blade, normal-to-the-blade, and spanwise.

Table 1. GRID DIMENSIONS

grid	type	no.	dimensions	pts. per grid	total pts.
duct	h	2	37x51x46	69,782	139,564
rotor	h	2	124x51x46	290,904	581,808
rotor	o	2	351x41x46	661,986	1,323,972
rotor	cl	2	351x12x5	21,060	42,120
stator	h	5	122x21x46	117,852	589,260
stator	o	5	351x31x46	500,526	2,502,630
total					5,179,305

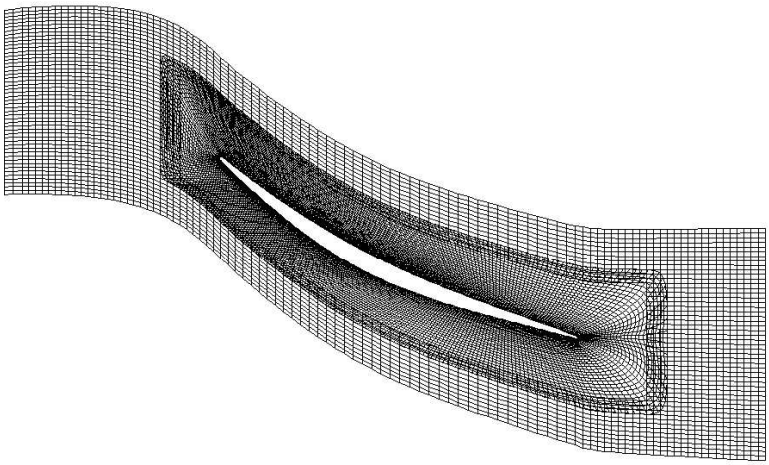

Figure 1. MIDSPAN SECTION OF ROTOR GRID.

Mid-span sections of the overset O- and H-grids for the rotor and stator are shown in Figs. 1 and 2 respectively.

The simulations were performed on an IBM p690 with 1.3 GHz Power4 processors. The domain was decomposed such that the solution for each H-grid and O-grid was performed on a separate processor, with the clearance grids on the same processors as their associated o-grids, for a total of 16 processors. Three dual-time-step iterations were performed for each global time step. Information was communicated between processors with MPI (Message Passing Interface). The simulation required approximately 65 seconds per global time step.

The flow conditions were provided in the form of a solution file from a similar simulation performed by NASA Glenn using APNASA, an average-passage turbomachinery flow solver. Once

Copyright © 2007 by ASME

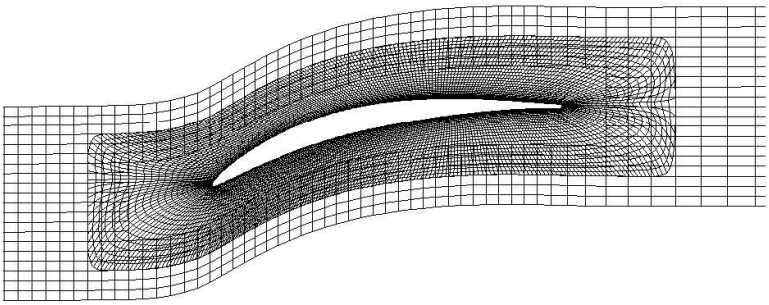

Figure 2. MIDSPAN SECTION OF STATOR GRID.

transients in the present simulation had settled down, the mass flow was calculated to verify the correct operating condition. The corrected mass flow in the present simulation was 58.01 lbm/s, which is close to the experimental value of 58.25 lbm/s [28].

For the current case, experimental data are limited to LDV velocity measurements in a plane perpendicular to the axis of the rig, 3.125 inches aft of the rotor tip trailing edge. The experimental data were not referenced to a specific circumferential location with respect to the fan blades, so in order to compare the simulations and the data, the wakes were shifted circumferentially so they were in the same locations. The resulting axial wake profiles at 10%, 30%, 50%, 70%, and 90% span are shown in Figs. 3 – 7, comparing the current simulation with both the experimental data and the APNASA simulation. The two simulations tend to over-predict or under-predict the wake deficit in different locations. The current simulation shows better prediction of the "freestream" velocity, and a more accurate wake profile.

ACOUSTIC METHOD

Acoustic propagation in an annular cylinder with uniform axial flow, can be computed using the method described in [5](pg. 65). A summary of the method as it is applied in this work is given here.

The acoustic computation is performed in the frequency domain. As such, the unsteady pressure is transformed using

$$p_\omega(\mathbf{x},\omega) = \frac{1}{2\pi}\int_{-\infty}^{\infty} p(\mathbf{x},t)e^{i\omega t}dt \quad (1)$$

$$p(\mathbf{x},t) = \int_{-\infty}^{\infty} p_\omega(\mathbf{x},\omega)e^{-i\omega t}d\omega \quad (2)$$

Application of Green's theorem inside the duct provides a

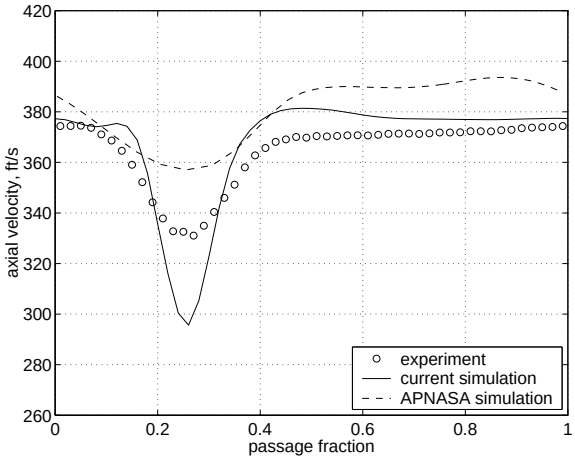

Figure 3. AXIAL WAKE PROFILE, 10% SPAN

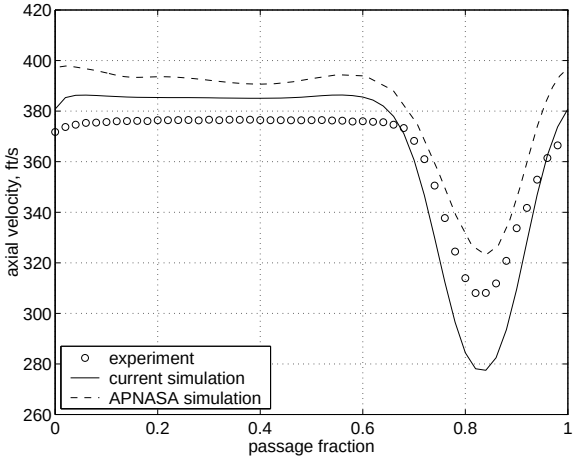

Figure 4. AXIAL WAKE PROFILE, 30% SPAN

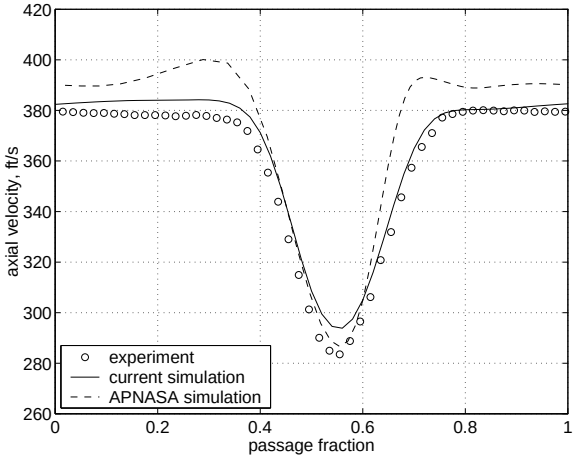

Figure 5. AXIAL WAKE PROFILE, 50% SPAN

Copyright © 2007 by ASME

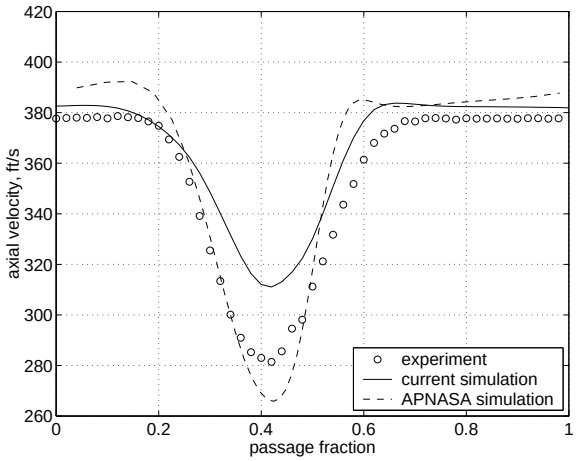

Figure 6. AXIAL WAKE PROFILE, 70% SPAN

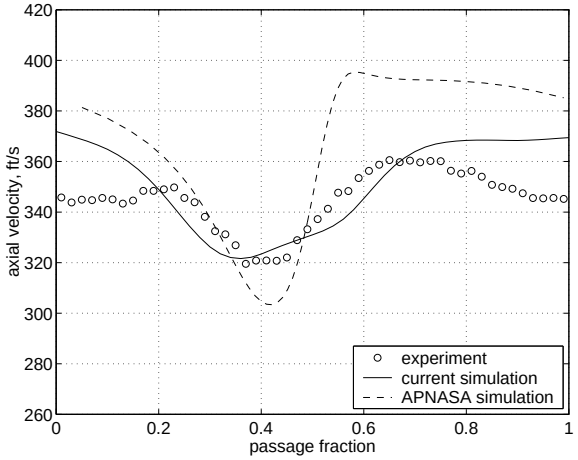

Figure 7. AXIAL WAKE PROFILE, 90% SPAN

method for computing the pressure at any point in the duct due the pressure on a vane or a set of vanes.

$$p_\omega(\mathbf{x},\omega) = -\int_S p_\omega(\mathbf{x_0},\omega)\frac{\partial}{\partial n}G_\omega(\mathbf{x_0}|\mathbf{x},\omega)dS(\mathbf{x_0}) \tag{3}$$

$$G_\omega = \sum_{n=-\infty}^{\infty}\sum_{m=0}^{\infty}\frac{i}{4\pi}\frac{e^{in(\theta-\theta_0)}}{\Gamma_{nm}(K_{nm}a)}\frac{\Psi_{nm}(K_{nm}r)\Psi_{nm}(K_{nm}r_0)}{\sqrt{k^2-\beta^2K_{nm}^2}}\times$$

$$exp[iMk(z_0-z)/\beta^2 + i\sqrt{k^2-\beta^2K_{nm}^2}|z_0-z|/\beta^2] \tag{4}$$

where $k=\omega/c_0$ and

$$\Psi_{nm}(K_{nm}r) = J_n(K_{nm}r) + Q_{nm}Y_n(K_{nm}r)$$

$$\Gamma_{nm}(K_{nm}a) = \int_h^a \left(J_n(K_{nm}r) + Q_{nm}Y_n(K_{nm}r)\right)^2 rdr$$

J_n and Y_n are Bessel functions order n of the 1st and 2nd kind, and K_{nm}, Q_{nm} are selected such that they satisfy the hard wall boundary condition ($\frac{\partial p}{\partial n}G_\omega = 0$) for the annulus

$$J_n'(K_{nm}a) + Q_{nm}Y_n'(K_{nm}a) = 0 \tag{5}$$
$$J_n'(K_{nm}h) + Q_{nm}Y_n'(K_{nm}h) = 0 \tag{6}$$

The Green's function provides insight into the acoustic modes that will propagate in the duct. In particular, the relation

$$k^2 > \beta^2K_{nm}^2 \tag{7}$$

must hold. Therefore, for each Fourier component, defined by ω, only a finite set of circumferential modes, defined by n, and radial modes, defined by m, will propagate. The other modes relate to evanescant waves that decay exponentially.

The radiated power at the inlet and at the exhaust were measured experimentally. The power at a given location in the duct is computed by integrating the intensity over the cross section of the duct such that

$$\mathcal{P} = \int_A \bar{\mathbf{I}}_t\cdot\hat{n}\; r\; drd\theta \tag{8}$$

where

$$\bar{\mathbf{I}}_t\cdot\hat{n} = (1+M^2)p(t)u(t) + \frac{M}{\rho_0c_0}p^2(t) + \rho_0c_0Mu^2(t) \tag{9}$$

[5](pg 201). A suitable expression for the axial unsteady velocity is obtained using the momentum equation below and Eq. (3)

$$\frac{\partial p_\omega}{\partial z} = \rho c_0\left(ik - M\frac{\partial}{\partial z}\right)u_\omega \tag{10}$$

to give

$$u_\omega = -\frac{1}{\rho_0c_0}\left[\frac{Mk\pm\sqrt{k^2-\beta^2K_{mn}^2}}{k\pm M\sqrt{k^2-\beta^2K_{mn}^2}}\right]p_\omega \tag{11}$$

Copyright © 2007 by ASME

where $\pm$ signifies if the point of interest is upstream (+) or downstream (-) of the disturbance.

In terms of the computed frequency-domain values of pressure and acoustic velocity, the expression for $\bar{\mathbf{I}}_t \cdot \hat{n}$ can be written as $(1+M^2)Real(p_\omega u_\omega^*)/2 + \dfrac{M}{\rho_0 c_0}|p_\omega|^2/2 + \rho_0 c_0 M|u_\omega|^2/2$.

Acoustic validation

The method for calculating the acoustic field due to the unsteady vane response has previously been validated. For instance, Nallasamy and Envia [19] used this method in conjunction with their recomputed unsteady vane surface pressures. Sutliff et al. [29] used experimental unsteady surface pressure data as input to the acoustic calculation and compared the acoustic field results to measurements. In both cases, the acoustic field results are reasonable and most trends are reproduced. Given the inherent limitations of the acoustic method (uniform axial flow, infinite cylindrical or annular duct) the results are quite good.

While the method has been validated, in order to determine if the current implementation of the method is correct, a validation test was considered. The cascade in distorted flow described by Hanson [30] was selected for the validation. The problem put forward as part of the 3rd Workshop on Aeroacoustic Benchmark problems is a three-dimensional flat-plate rotor configuration with 24 vanes (V) interacting with an inlet distortion related to 16 blades (B). The solution to the problem was presented by Namba and Schulten [31].

In the benchmark problem, the nondimensional stator chord is constant along the span at c/r_t = 0.2618, the relative Mach number at each radial location is 0.5, the hub-to-tip ratio is 0.5, there is no stagger, and the gap-to-chord ratio is 1.0 at the tip. The case we consider here has a rotor tip Mach number of $M_t = 0.783$. Solutions to the benchmark problem were reported in terms of the complex coefficients of the pressure field modal expansion

$$p(r,\theta,x,t) = p_0 \sum_{k=-\infty}^{\infty} \sum_{m=0}^{\infty} A_{nm}(x)\Psi_{nm}(r)e^{i(n\theta-\omega t)} \qquad (12)$$

where the circumferential modes of interest are restricted by the relation $n = qB - sV$ (where q and s are integers).

The cut-on/cut-off criterion is given by Eq. (7). For the benchmark problem, the acoustic wave number is given as $k = \dfrac{\omega}{c_0} = \left(\dfrac{qB}{a}\right)\left(\dfrac{a\Omega}{c_0}\right) = \dfrac{qBM_t}{a}$. If the duct were a cylinder, one could approximate the eigenfrequencies from the boundary condition equation, $J_n'(K_{nm}a) = 0$, as $K_{nm} \sim n/a$. Thus, an approximation for the the cut-on criteria would be

$$\frac{M_t}{\beta} > \frac{|(qB - sV)|}{|qB|} = \left|\frac{n}{qB}\right| \qquad (13)$$

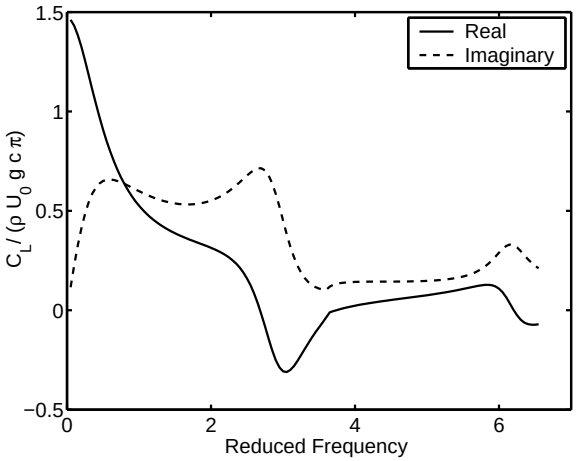

Figure 8. SECTION COEFFICIENT OF LIFT (L/($\pi\rho_0 U_0 gc$) VS. REDUCED FREQUENCY ($\omega c/(2U_0)$). TWO-DIMENSIONAL CASCADE, 16 ROTORS, 24 VANES, M = 0.5, SPACING = 1.0, STAGGER =0.

The benchmark problem is only concerned with the first blade passage frequency, $q = 1$. Therefore, one finds that only $n = -8$, which coresponds to $s = 1$, propagates.

For the blade passage frequency considered in the benchmark problem, with a cylindrical mode of n = -8, the eigenfrequencies for the first four radial modes for the hub-to-tip ratio of 0.5 and Mach number of 0.5, are -9.64, -13.8, -17.344, -22.136. One can see that the approximation of -8 used above for the first eigenfrequency is reasonable. The corresponding Q_{nm} values are -0.0046, -0.2652, -0.4047, 1.1206.

In the present simulation, the unsteady pressure on the blade is calculated using a strip theory. The response of a two-dimensional, unloaded, flat-plate cascade to a gust is computed at each strip via the method of Ventres [7].

The response of a single strip is consistent with the two-dimensional results reported in [31]. The current results for the 2D section coefficient of unsteady lift, which are identical to those given in [31], are shown in Fig. 8.

For the current 3D simulation, the specifications for each 2D strip were: k_1 = 3.279, $M = 0.5$, stagger = 0, intervane phase angle = 4.1887, gap-to-chord = r (radial location), k_2 = 4.1887/gap-to-chord. (Here the reduced frequencies are normalized by the half-chord). The unsteady surface pressure on the blade is shown in Figs. 9 and 10. This unsteady pressure was used to calculate the modal amplitude of the pressure one chord length upstream and one chord length downstream as per the benchmark problem statement. The complex amplitudes from the current simulation and those reported in [31] are given in Table 2 at the end of the paper. The discrepancies in the results stem from the fact that the strip theory results match the lifting surface results reported in [31] in the mid-span region, however, they vary greatly at both the hub and tip. Thus, true validation of the acoustic computation

Copyright © 2007 by ASME

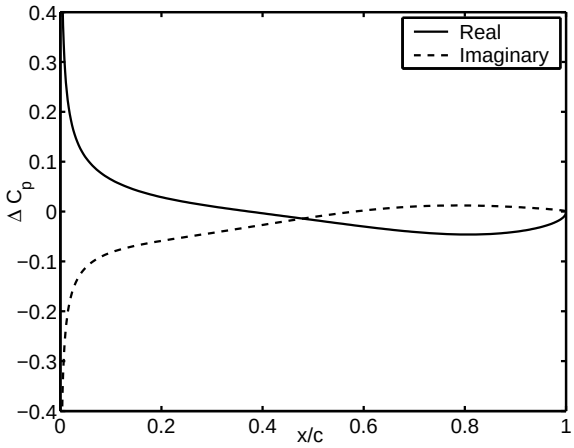

Figure 9. REAL AND IMAGINARY PARTS OF THE UNSTEADY STATOR SURFACE PRESSURE AT THE CENTERSPAN $\omega c/(2U) = 6.56, M = 0.5$.

cannot be completed using the strip theory method for computing the surface pressure.

Results

The computation of the sound generated downstream by the exit guide vanes in the NASA STD 22 rotor, 54 vane case is the focus of this research. In order to increase the speed of the turbomachinery flow computation, the actual periodic blade count 11:27 that would be needed to exactly represent the experimental setup was approximated using a 2:5 count. The spacing between the rotor and stator is 2.5 tip chords.

The plot of the entropy throughout the entire grid, Fig. 11, allows one to visualize the rotor-wake interaction with the stators. The rotor wakes provide the unsteady forcing on the vanes. Qualitative comparison of the wakes with those presented in [19] is possible. Figure 12 shows the axial velocity approximately 0.2 axial chords behind the fan rotor. The wakes are clearly defined, and the region of interaction between the tip clearance flow and the main flow is also apparent.

Fig. 13 shows the time trace of the surface pressure on a representative stator vane for a point located at mid-span near the leading edge.There is a low frequency component visible that might be a transient that has not completely decayed. Because it is at such a low frequency, it does not effect the present simulations. The pressure is normalized by the upstream static pressure. Six blade passages were used to obtain the transform of the pressure. The FFT is shown in Fig. 13

This study focuses on the tonal noise from the interaction of the stators with the rotor wakes. The BPF is at $2\pi\Omega$ B. The true rotor speed was 7921 rpm giving a blade passage frequency of 18.249 kHz. Therefore $2\times$ BPF is at 36.498 kHz. The real part

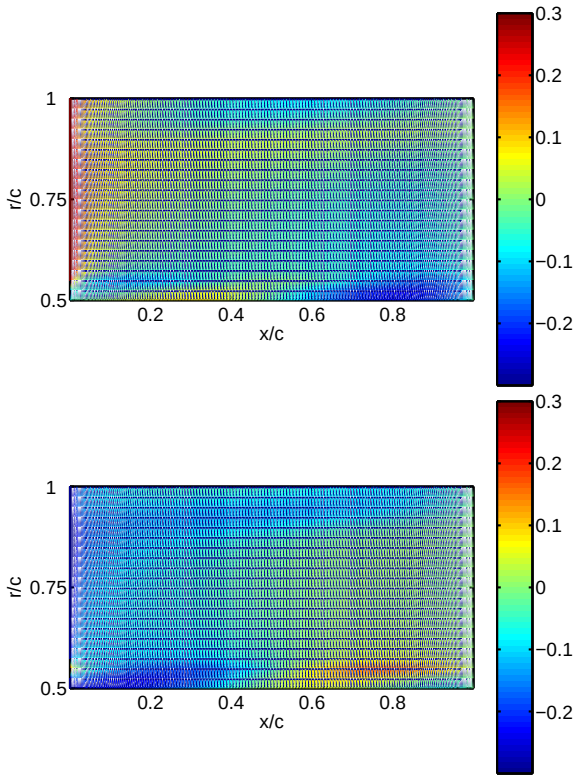

Figure 10. REAL (TOP) AND IMAGINARY (BOTTOM) PARTS OF THE UNSTEADY STATOR SURFACE PRESSURE $\omega c/(2U) = 6.56, M = 0.5$.

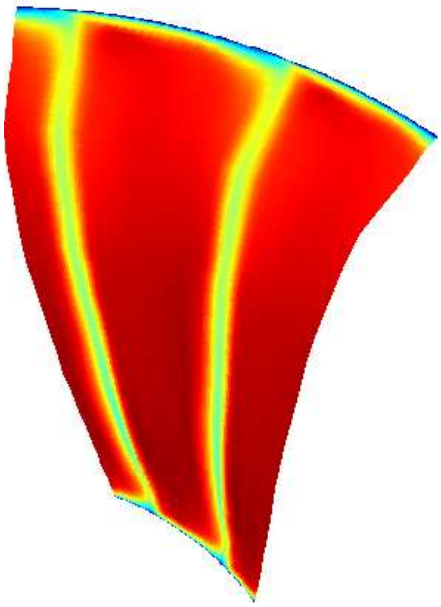

Figure 12. AXIAL VELOCITY APPROXIMATELY 0.2 AXIAL CHORDS BEHIND THE FAN BLADE.

Copyright © 2007 by ASME

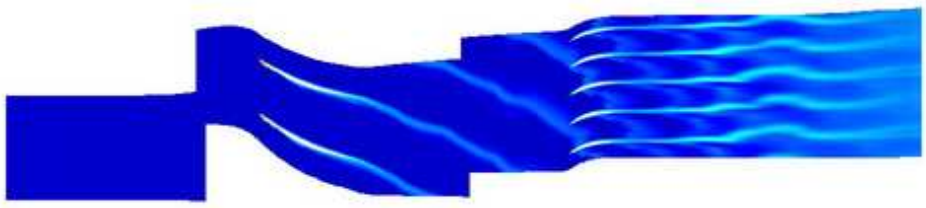

Figure 11. ENTROPY.

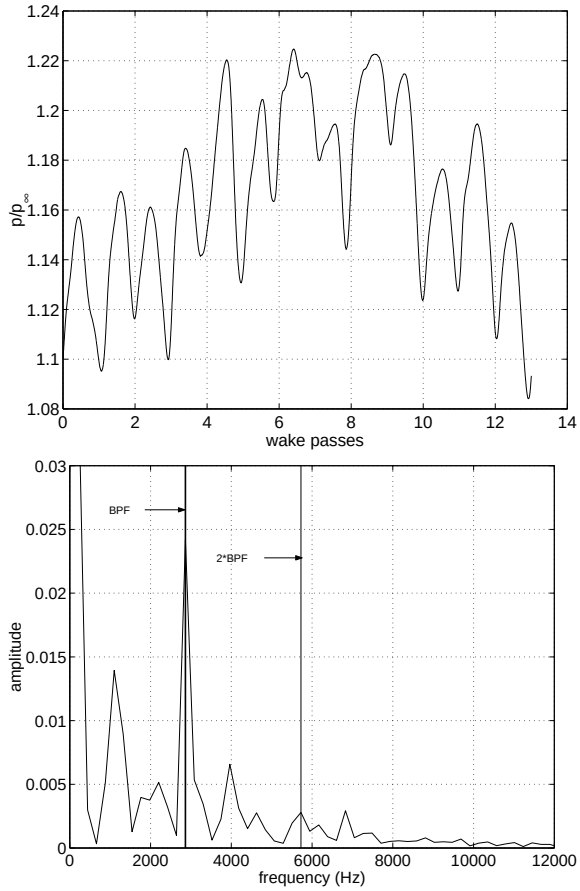

Figure 13. PRESSURE VS. TIME (TOP) AND PRESSURE VS. FREQUENCY (BOTTOM) AT A POINT NEAR THE LEADING EDGE OF THE STATOR VANE MIDSPAN.

of the nondimensional surface pressure at the first and second blade passage frequencies is shown in Fig. 14. The real and imaginary parts of the pressure along the centerspan for the two frequencies of interest are shown in Fig. 15.

The acoustic model assumes an annular duct with constant cross-section and uniform axial flow. In addition, the surface pressure on a single vane is recorded from the CFD solution. It is assumed that all of the stator vanes have the same pressure adjusted by the inter-vane phase angle.

A sketch of the real duct geometry is shown in Fig. 16. For the simulation, the duct downstream of the rotor is chosen to match the duct geometry at the leading edge of the stator vane. Thus, it does not conform to the geometry at the exhaust plane. Eq. (13), states that for this case where $k = 2.376$ (nondimensional), there is no value of s when $q = 1$ for which the relation can hold. Thus, for the BPF all modes are cut off. However, when $q = 2$, $s = 1$ satisfies the relation and thus circumferential mode $n = -10$ is cut on.

The experimental power levels that are used for comparison here were obtained using a rotating rake [32] installed at the exhaust plane. The experiment confirmed that there was no dominant interaction mode at BPF and at 2 BPF the $n = -10$ mode contained most of the energy. The power level for the $n = -10$ mode was almost 115 dB (reference 10^{-12}). Other modes did contribute minor amounts to the total tone power levels measured experimentally. This simulation, which does not include the variable duct geometry and simulates the difference in surface pressure from vane-to-vane via only the inter-vane phase angle, does not allow other modes to propagate to the exhaust plane. For the 2 BPF case, the simulation predicts that the exhaust plane power level for n = -10 is 117.9 dB. That this value is slightly higher than the experimental value, maybe due to the fact that our simulated exhaust plane is larger than the real exhaust plane. The excellent agreement with experiment here is exciting and motivates further validation of the method.

Conclusion

A 3-D, unsteady, Reynolds-averaged Navier-Stokes CFD code was used to predict the fully coupled turbomachinery flow field and vane surface pressures for a geometry consistent with the NASA 22 inch fan rig. The vane unsteady surface pressures were then used in conjunction with an analytical duct acoustic model to predict the tonal sound power level at the exhaust plane. Although the acoustic model did not include the varying duct cross section, nor any small vane-to-vane pressure differences (not related to the intervane phase angle), the prediction of the

Copyright © 2007 by ASME

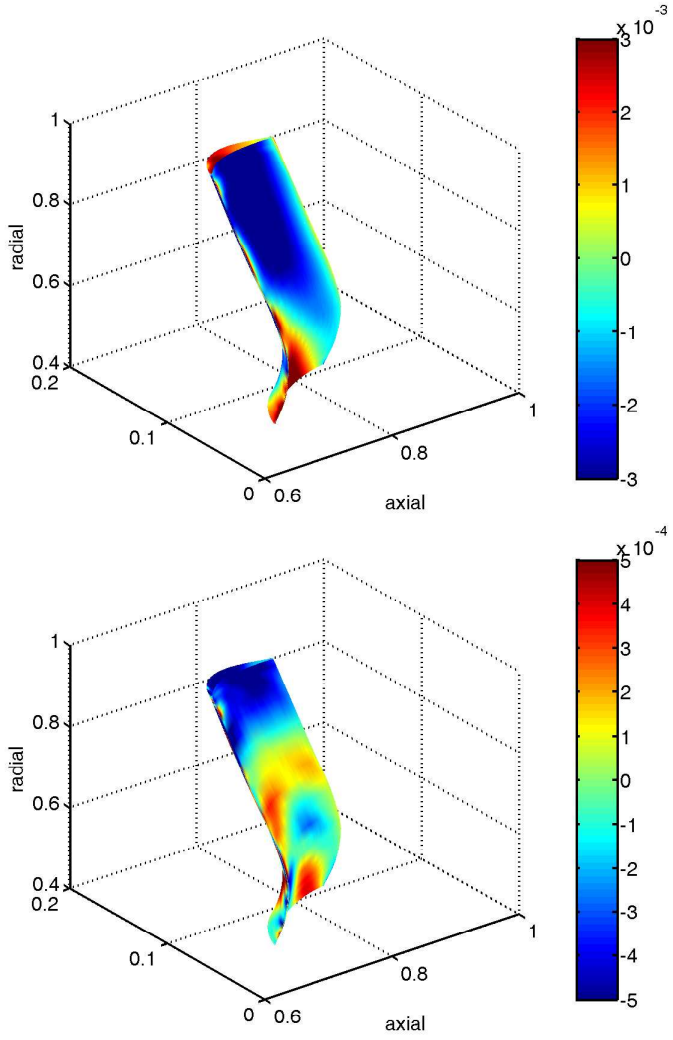

Figure 14. REAL PART OF THE UNSTEADY PRESSURE ON THE STATOR VANE, AT BPF (TOP) AND 2 BPF (BOTTOM).

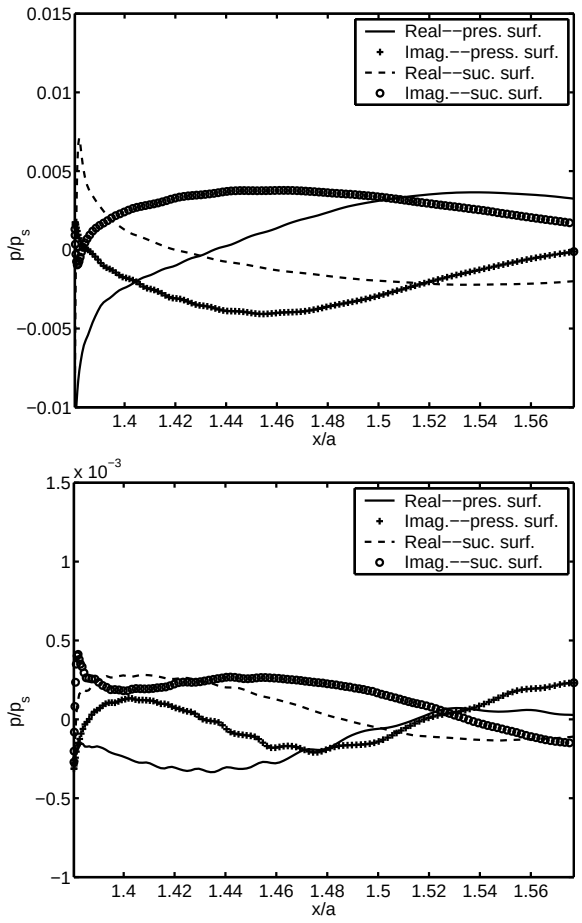

Figure 15. REAL PART OF THE UNSTEADY PRESSURE ALONG THE CENTERSPAN OF THE STATOR VANE, AT BPF (TOP) AND 2 BPF (BOTTOM).

sound power associated with the one propagating wave associated with the second blade passage frequency was outstanding.

The present result motivates further investigations to determine if the acoustic model can be extended to accurately include the effect of varying duct cross section. In addition, the contribution of other non BPF associated frequencies to the overall sound power will be studied. The correspondance of these other frequencies with broadband noise will be considered. Finally, an additional fan configuration from the NASA test, for which there are experimental vane surface pressure data available will be run.

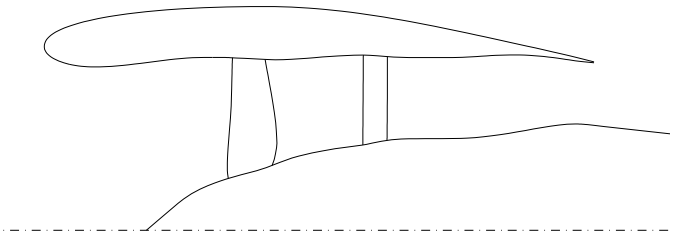

Figure 16. FLOW PATH OF THE EXPERIMENTAL RIG.

ACKNOWLEDGMENT

The authors would like to thank Dr. E. Envia of NASA Glenn for providing the relevant experimental test specifications

Copyright © 2007 by ASME

	Upstream Wave, $x = -c$					
	n = -8					
	Real			Imaginary		
	Namba	Schulten	Current	Namba	Schulten	Current
m = 0	3.493E-03	5.140E-03	4.2207E-2	1.125E-02	1.056E-02	4,5616E-2
m = 1	06.674E-03	-7.631E-03	2.1678E-2	-1.811E-02	-1.747E-02	-2.2627E-1
m = 2	-1.816E-04	-8.145E-05	-1.676E-3	1.243E-04	1.072E-04	-1.2537E-3
m = 3	-3.028E-06	-1.370E-06	2.4204E-5	4.329E-06	4.021E-06	2.4821E-5
	Downstream Wave, $x = +2c$					
	n = -8					
	Real			Imaginary		
	Namba	Schulten	Current	Namba	Schulten	Current
m = 0	-1.707E-02	-1.497E-02	-1.5487E-1	-1.594E-03	-2.731E-04	-3.5859E-2
m = 1	7.702E-03	8.603E-03	-1.4593E-2	1.731E-02	1.564E-02	5.8392E-2
m = 2	1.022E-04	1.729E-04	2.3565E-3	-1.558E-04	-2.034E-04	-6.7854E-4
m = 3	1.589E-06	3.048E-06	2.4204E-5	-2.310E-06	-3.024E-06	-2.3440E-5

Table 2. COMPLEX AMPLITUDE OF ACOUSTIC WAVES FOR VALIDATION. n IS CIRCUMFERENTIAL MODE NUMBER, m IS RADIAL MODE NUMBER.

and data and discussing the testing and related simulation work.

REFERENCES

[1] Podboy, G. G., and Helland, S. M., 2002. "Fan noise source diagnostic test-two-point hot-wire results". In AIAA Paper 2002-2431, AIAA.

[2] Woodward, R. P., 2002. "Fan noise source diagnostic test-farfield acoustic results". In AIAA Paper 2002-2427, AIAA.

[3] Hanson, D. B., and Horan, K. P., 1998. "Turbulence/cascade interaction – spectra of inflow, cascade response, and noise". *AIAA Paper No. 98-2319*. 4th AIAA/CEAS Aeroacoustics Conference.

[4] Ganz, U., Glegg, S., and Joppa, P., 1998. "Measurement and prediction of broadband fan noise". In Proceedings of the 4th AIAA/CEAS Aeroacoustics Conference. Paper no. AIAA-98-2316.

[5] Goldstein, M. E., 1976. *Aeroacoustics*. McGraw-Hill International Book Co., New York, etc.

[6] Namba, M., 1977. "Three-dimensional analysis of blade force and sound generation for an annual cascade in distorted flows". *Journal of sound and vibration,* **50**(4), pp. 479–508.

[7] Ventres, C., Theobald, M. A., and Mark, W. D., 1982. Turbofan noise generation volume 1: Analysis. Tech. Rep. CR-167952, NASA, July.

[8] Hall, K. C., and Verdon, J. M., 1991. "Gust response analysis for cascades operating in nonuniform mean flows". *AIAA Journal,* **29**(9), pp. 1463–1471.

[9] Fang, J., and Atassi, H., 1993. "Direct calculation of sound radiated from a loaded cascade of loaded airfoils". In proceedings of Computational Aero- and Hydro-Acoustics, ASME FED, Vol. 147, pp. 111–116.

[10] Majumdar, S. J., and Peake, N., 1996. "Three-dimensional effects in cascade-gust interaction". *Wave Motion,* **23**(4), pp. 321–337.

[11] Hanson, D. B., 1999. "Influence of lean and sweep on noise of cascades with turbluent inflow". *AIAA Paper No. 99-1863*. 5th AIAA/CEAS Aeroacoustics Conference.

[12] Atassi, H. M., Fang, J., and Patrick, S. M., 1993. "Direct calculation of sound radiated from bodies in nonuniform flows". *Journal of Fluids Engineering,* **115**, December, pp. 573–579.

[13] Peake, N., and Kerschen, E. J., 2004. "Influence of mean loading on noise generated by the interaction of gusts with

Copyright © 2007 by ASME

a cascade: downstream radiation". *Journal of Fluid Mechanics,* **515**, pp. 99–133.

[14] Peake, N., and Kerschen, E. J., 1997. "Influence of mean loading on noise generated by the interaction of gusts with a cascade: upstream radiation". *Journal of Fluid Mechanics,* **347**, pp. 315–346.

[15] Cooper, A. J., and Peake, N., 2001. "Propagation of unsteady disturbances in a slowly varying duct with mean swirling flow". *Journal of Fluid Mechanics,* **445**, pp. 207–234.

[16] Golubev, V. V., and Atassi, H. M., 2000. "Unsteady swirling flows in annular cascades, part 1: aerodynamic blade response". *AIAA Journal,* **38**(7), pp. 1150–1158.

[17] Golubev, V. V., and Atassi, H. M., 2000. "Unsteady swirling flows in annular cascades, part 1: evolution of incident disturbances". *AIAA Journal,* **38**(7), pp. 1142–1149.

[18] Heaton, C. J., and Peake, N., 2005. "Acoustic scattering in a duct with mean swirling flow". *Journal of Fluid Mechanics,* **540**, pp. 189–220.

[19] Nallasamy, M., and Envia, E., 2005. "Computation of rotor wake turbulence noise". *Journal of Sound and Vibration,* **282**, pp. 649–678.

[20] Saren, V. E., Savin, N. M., Dorney, D. J., and Sondak, D. L., 1998. "Experimental and numerical investigation of airfoil clocking and inter-blade-row gap effects on axial compressor performance". *International Journal of Turbo and Jet Engines,* **15**, pp. 235–252.

[21] Dorney, D. J., and Davis, R. L., 1992. "Navier-stokes analysis of turbine blade heat transfer and performance". *ASME Journal of Turbomachinery,* **114**(4), pp. 795–806.

[22] Sondak, D. L., and Dorney, D. J., 2003. "General equation set solver for compressible and incompressible turbomachinery flows". *AIAA 2003-4420*.

[23] Venkateswaran, S., and Merkle, C. L., 1999. "Analysis of preconditioning methods for euler and navier-stokes equations". In *von Karman Institute Lecture Series*. May.

[24] Roe, P. L., 1981. "Approximate riemann solvers, parameter vectors and difference schemes". *Journal of Computational Physics,* **43**, pp. 357–372.

[25] Baldwin, B. S., and Lomax, H., 1978. "This layer approximation and algebraic model for separated turbluent flows". *AIAA Paper 78-257*.

[26] Dorney, D. J., and Sondak, D. L., 2000. "Three-dimensional simulations of airfoil clocking in a 1-1/2 stage turbine". *AIAA Paper 2000-3359*.

[27] Dorney, D. J., and Sondak, D. L., 2000. "Effects of tip clearance on hot streak migration in a high-subsonic single-stage turbine". *ASME Journal of Turbomachinery,* **122**, pp. 613–620.

[28] Hughes, C. E., 2007. private communication.

[29] Sutliff, D. L., Heidelberg, L. J., and Envia, E., 1999. "Coupling of low speed fan stator vane unsteady pressure to duct modes: Measured vs. predicted". *AIAA-99-1864*.

[30] Hanson, D. B., 2000. "Category 4 – fan stator with harmonic excitation by rotor wakes". In Third Computational Aeroacousitcs (CAA) Workshop on Benchmark Problems, NASA/CP–2000-2090790, pp. 17–20.

[31] Namba, M., and Schulten, J. B. H. M., 2000. "Numerical results of lifting surface theory". In Third Computational Aeroacousitcs (CAA) Workshop on Benchmark Problems, NASA/CP–2000-2090790, pp. 73–85.

[32] Heidelberg, L. J., 2002. "Fan noise source diagnostic test-tone modal structure results". In AIAA Paper 2002-2428, AIAA.

Copyright © 2007 by ASME